Journal of Inorganic and General Chemistry

ZAAC

Zeitschrift für anorganische und allgemeine Chemie

Accepted Article

Title: Synthesis, Crystal Structure and Magnetic Properties of K6Mn4O7 Featuring a Novel Two-Dimensional Poly-oxomanganate(II) Anion

Authors: Martin Jansen, Jürgen Nuss, and Reinhard Kremer

To be cited as: *Z. anorg. allg. Chem.* 10.1002/zaac.201800169

Link to VoR: http://dx.doi.org/10.1002/zaac.201800169

WILEY-VCH

www.zaac.wiley-vch.de

10.1002/zaac.201800169

WILEY-VCH

ARTICLE

Synthesis, Crystal Structure and Magnetic Properties of $K_6Mn_4O_7$ Featuring a Novel Two-Dimensional Poly-oxomanganate(II) Anion

Jürgen Nuss,[a] Reinhard K. Kremer,[a] and Martin Jansen*[a]

Dedicated to Professor Wolfgang Bensch on the Occasion of his 65th Birthday

Abstract. $K_6Mn_4O_7$ has been synthesized via the azide/nitrate route from a stoichiometric mixture of the precursors KN_3, KNO_3, and MnO, and alternatively from the binary constituents K_2O and MnO, in an all-solid state reaction. Its crystal structure [$P\bar{1}$, Z = 1, a = 603.46(3), b = 647.69(4), c = 891.36(5) pm, α = 90.477(2)°, β = 108.417(2)°, γ = 115.358(2)°] consists of cluster-like Mn_4O_{10} units, each composed by four edge sharing MnO_4 tetrahedra. The Mn_4O_{10} building blocks, on their part, are linked by six vertices, forming a 2D arrangement, ${}^{2}_{\infty}[Mn_4O_{4/1}O_{6/2}]^{6-}_{n}$, with the potassium cations occupying the space in between. The temperature dependence of the magnetic susceptibility is dominated by antiferromagnetic coupling along a low-dimensional magnetic exchange path. The heat capacity reveals no clear sign of long-range magnetic ordering supporting an interpretation of $K_6Mn_4O_7$ as a new low-dimensional magnetic system.

Introduction

Due to their anisotropic magnetic and electronic properties low dimensional arrangements of open shell transition elements continue to be in the focus of condensed matter research. Charge, spin, orbital and structural degrees of freedom on such (sub-) lattices are relevant ingredients for the evolution of sought-after bulk functionalities like magnetoresistance or superconductivity. Although known for decades, these macroscopic phenomena are still not fully understood on the microscopic level. Indeed, the heavily entangled degrees of freedom mentioned above give rise to a virtually indigestible complexity, which is aggravated by the fact that the periodicities of most of such materials are often significantly perturbed, undermining rigorous theoretical treatment and obscuring experimental response.[1]

One option to reduce the complexity would be to lift part of the degrees of freedom. In pursuing this thought, we have started to investigate oxide systems that show charge, spin and orbital ordering, however, on a fully periodic lattice and with defined valence states of the transition metals involved. Among the candidates realized are intrinsically doped sodium cuprates(II,III), Na_xCuO_2,[2-10] featuring strands of trans-edge sharing CuO_4 squares. The respective *quasi* 1D cuprate anions have furnished plenty of particular ordering schemes; among others, they represent unequivocal manifestations of Wigner crystallization,[4] are magnetically frustrated,[6-8] or undergo magnetic excitations across the Wigner gap.[10] As a similarly relevant class of compounds, alkali metal manganates(II,III) of general composition A_xMnO_2 (A = K, Rb, Cs; $1 \leq x \leq 2$)[11-16] have become available through the azide/nitrate route of synthesis.[17,18]

In order to exclude charge ordering as one of the degrees of freedom we were striving for low dimensional manganates containing manganese in an integral oxidation state, e.g. of 2+. In accordance with the particular stability of the half-filled *d*-shell, this oxidation state is regarded a quite common one for manganese. However, the number of alkali metal oxomanganates(II) reported has remained surprisingly low. The main obstacle to the synthesis of such ternary oxides is the pronounced inclination of manganese to undergo oxidation during solid state reactions involving strongly basic alkali metal oxides. This implication has been overcome in singular cases by using closed reaction vessels made of reducing materials or, in a more rational fashion, by applying the azide/nitrate route.[17,18] While some sodium manganates(II), as there are Na_2MnO_2,[19] $Na_2Mn_2O_3$,[20] or Na_6MnO_4,[21] have been reported, ternary oxomanganates(II) of the heavier alkali metals are quite rare. Here, $Cs_{23}Mn_{16}O_{28}$,[22] still contains one Mn^{3+} species per formula unit, and $Rb_2Mn_3O_4$[23] and $K_2Mn_2O_3$[24] are the only rubidium and potassium oxomanganates(II) known, so far.

Here we report on synthesis, structure determination, and physical properties of $K_6Mn_4O_7$, displaying strong antiferromagnetic exchange coupling on a two-dimensional novel poly-oxomanganate(II) grid.

Results and Discussion

Synthesis

$K_6Mn_4O_7$ was discovered by chance as an impurity phase during our investigations of the K_xMnO_2 system.[11,16] Subsequently, the title compound was synthesized along the azide/nitrate route[17,18] as a single phase material. Alternatively, conventional solid state synthesis from the binary oxides K_2O and MnO has been shown to be viable, as well. The transparent, orange product is very sensitive to humid air. The powder X-ray diffraction pattern is shown in Figure 1.

* Prof. Dr. Dr. h.c. M. Jansen
E-mail: M.Jansen@fkf.mpg.de
[a] Max-Planck-Institut für Festkörperforschung
Heisenbergstraße 1
70569 Stuttgart
Germany

10.1002/zaac.201800169

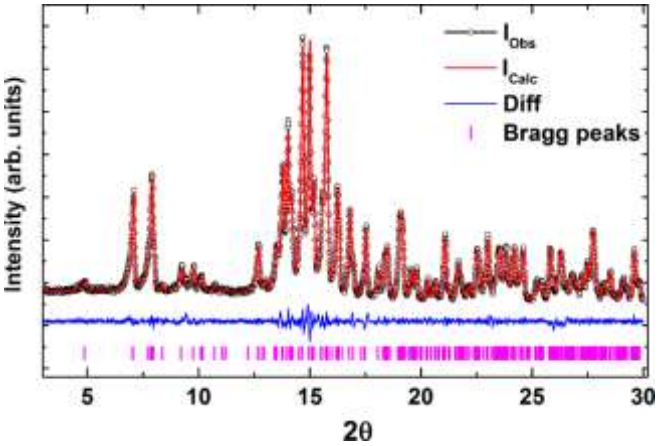

Figure 1. PXRD pattern of $K_6Mn_4O_7$ and corresponding Le Bail fit, at 298 K. The difference plot is drawn below the profile; tick marks indicate peak positions of the $K_6Mn_4O_7$ compound.

Crystal Structure

According to single-crystal X-ray structure analysis, $K_6Mn_4O_7$ displays an unprecedented crystal structure, Pearson code *aP*17. Details on data collection, structural parameters, atomic coordinates, and displacement parameters are given in Tables 1 and 2.

Table 1. Crystal data, data collection and refinement details for $K_6Mn_4O_7$ at 298 K.

Formula weight	598.04	
Space group (no.), *Z*	$P\bar{1}$ (2), 1	
Lattice parameters[a] /pm, /°	a = 603.46(3) b = 647.69(4) c = 891.36(5)	α = 90.477(2) β = 108.417(2) γ = 115.358(2)
V /Å^3	294.48(3)	
ρ_{xray} /g×cm^{-3}	3.194	
Crystal size /mm^3	0.11×0.07×0.05	
Diffractometer	SMART APEX I, Bruker AXS	
X-ray radiation, λ /pm	MoKα, 71.073	
Absorption correction	Multi-scan, SADABS	
2θrange /°	4.88 ≤ 2θ ≤ 69.80	
Index ranges	–9 ≤ h ≤ 9, –10 ≤ k ≤ 10, –13 ≤ l ≤ 14	
Reflections collected	4595	
Data, R_{int}	2380, 0.015	
No. of parameters	79	
Transmission: t_{min}, t_{max}	0.414, 0.497	
R_1 [$F^2 > 2\sigma(F^2)$]	0.028	
wR(F^2)	0.070	
Deposition no.[b]	CSD-434446	

[a] Lattice parameters extracted from X-ray powder diffraction data.

[b] Further details of the crystal structure investigations may be obtained from the Fachinformationszentrum Karlsruhe, 76344 Eggenstein-Leopoldshafen, Germany (Fax: +49-7247-808-666; E-Mail: crysdata@fiz-karlsruhe.de, http://www.fiz-karlsruhe.de/request for deposited data.html) on quoting the depository number.

Table 2. Atomic coordinates and displacement parameter U_{eq} /pm^2 for $K_6Mn_4O_7$ at 298 K.

Atom	Site	*x*	*y*	*z*	U_{eq}
Mn1	2*i*	0.77696(5)	0.84337(5)	0.36611(3)	133.6(7)
Mn2	2*i*	0.11517(5)	0.89182(5)	0.20861(3)	121.4(7)
K1	2*i*	0.51073(9)	0.76462(9)	0.97296(6)	256(1)
K2	2*i*	0.68821(9)	0.28300(8)	0.45543(5)	224.9(9)
K3	2*i*	0.8768(1)	0.60350(8)	0.80895(6)	251(1)
O1	1*a*	0	0	0	169(3)
O2	2*i*	0.8482(3)	0.8751(2)	0.6069(2)	170(2)
O3	2*i*	0.4497(3)	0.8705(3)	0.2431(2)	205(3)
O4	2*i*	0.8288(3)	0.6026(2)	0.2489(2)	185(3)

The title compound constitutes a new oxomanganate(II). Similar to most of such alkali metal manganates reported earlier,[11-16,19-24], the Mn^{2+} cations are coordinated by four oxygen atoms forming strongly distorted MnO_4 tetrahedra, with bond lengths *d*(Mn—O) ranging from 201 to 215 pm, and angles ∠(O—Mn—O) from 94 to 122° (see Table 3). Four of these primary building units aggregate via edge sharing to a tetrameric, cluster-like building block of composition Mn_4O_{10} exhibiting point group symmetry $\bar{1}$, as a secondary substructure. The double-bended arrangement of this unique building block results in short contacts between manganese atoms *d*(Mn—Mn) of 274 to 288 pm, with angles ∠(Mn2—Mn1—Mn1) of 87.71(2)°, and an dihedral angle ∠(Mn2—Mn1—Mn1—Mn2) of 180° (see Table 3 and Figure 2).

Table 3. Selected interatomic distances and angles for $K_6Mn_4O_7$ at 298 K.

Atomic contact	Distance /pm	Atomic contact	Angle /°
Mn1—Mn1	287.08(6)	Mn2—O1—Mn2	180
Mn1—Mn2	273.94(4)	Mn1—O2—Mn1	86.45(5)

10.1002/zaac.201800169

Mn1—O2	204.2(1) 214.9(1)	Mn1—O2—Mn2	138.51(8) 79.96(5)
Mn1—O3	201.6(1)	Mn1—O3—Mn2	156.97(9)
Mn1—O4	205.4(1)	Mn1—O4—Mn2	83.44(5)
Mn2—O1	201.34(3)	O—Mn—O	93.55(6)-
Mn2—O2	211.5(1)		121.82(6)
Mn2—O3	200.9(1)		
Mn2—O4	206.2(1)		
K—O	254.6(2)-310.6(2)		

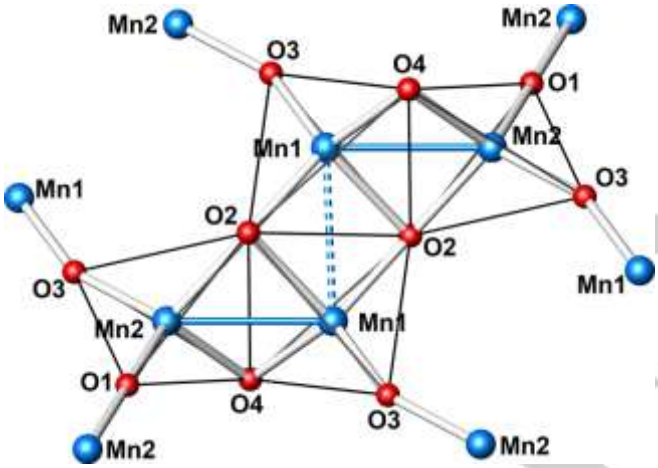

Figure 2. Tetrameric subunit of the $^{2}_{\infty}[Mn_4O_7]^{6-}_{n}$ layer. Colour code: oxygen (red spheres), manganese (blue spheres), edges of the MnO_4 tetrahedra (black lines), Mn—O bonds (white rods), shortest distances between manganese atoms are emphasized as blue sticks.

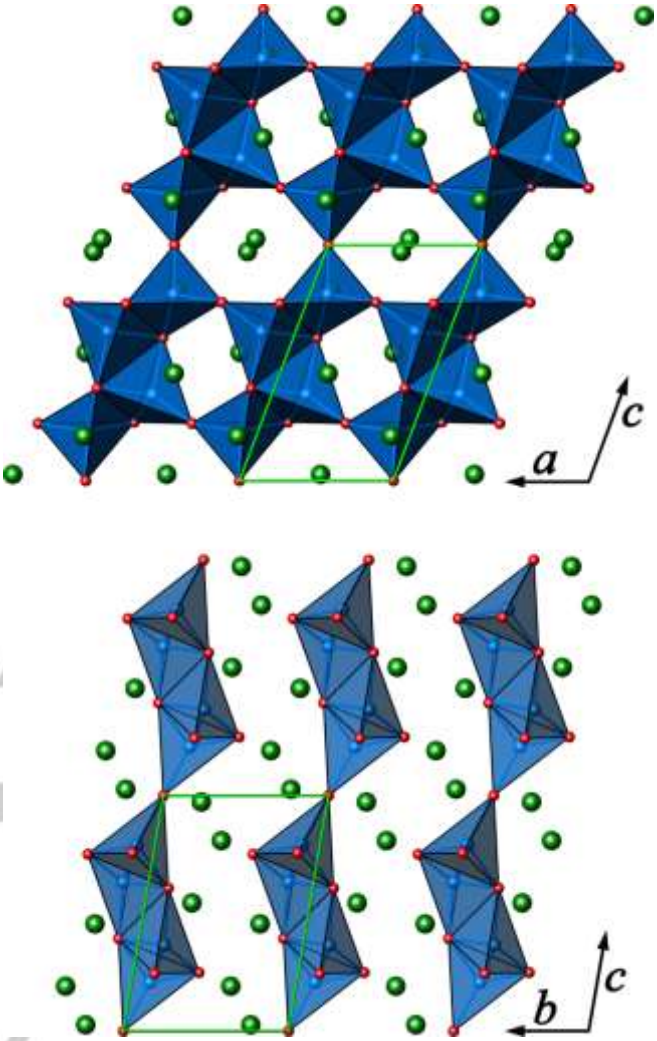

Figure 3. Projections of the crystal structure of $K_6Mn_4O_7$, with margins of the unit cell (green). (Top) view along [0 1 0], (bottom) view along [1 0 0]. Colour code: MnO_4 tetrahedra (blue), oxygen (red spheres), manganese (blue spheres), potassium (green spheres).

The Mn_4O_{10} building blocks, on their part, are linked by six vertices to form the tertiary two-dimensional grid, $^{2}_{\infty}[Mn_4O_7]^{6-}_{n}$, extending parallel to the *a-c* plane, see Figure 3. The potassium cations occupy the space between these layers with K—O distances ranging from 254 to 311 pm, and coordination numbers of 4 and 5.

From the specific connectivity pattern as exhibited by the 2D poly-oxoanion it is evident that the paths possible for magnetic exchange coupling are quite distinct, resulting in a set of complex magnetic interactions. Within the tetrameric subunit consisting of tetrahedra sharing common edges, weak ferromagnetic (FM) interactions will prevail, while the character of inter-cluster exchange coupling will be antiferromagnetic (AFM), however substantially different in strength, according to the spread in the respective Mn—O—Mn angles.[25,26]

Magnetic Properties

Figure 4 displays the magnetic susceptibility and the heat capacity of $K_6Mn_4O_7$. The magnetic susceptibility is characterized by a very broad hump centered at ~430 K and a rather steep upturn below ~35 K. The broad hump is characteristic for short-range antiferromagnetic correlations as typically observed in low

10.1002/zaac.201800169

dimensional magnetic systems. The low-temperature upturn may be ascribed to un-correlated magnetic moments due to defects or minute impurities. The heat capacity exhibits a tiny λ-type anomaly at ~117.5 K, which we tentatively ascribe to long-range magnetic ordering of a faint trace of a MnO impurities. The entropy covered by this anomaly amounts to ~0.1 J/mol K only i.e. ~0.5 % of the magnetic entropy, *R*ln6, expected for a spin *S* = 5/2 system pointing to an impurity concentration far below the detection limits of powder x-ray diffraction experiments. Absence of any further anomalies in the heat capacity supports our interpretation of $K_6Mn_4O_7$ as a low-dimensional magnetic system for which the magnetic heat capacity contribution due to short-range magnetic order spreads out over a wide temperature making it difficult to discern it from the lattice heat capacity. The majority of the magnetic entropy has already been removed by short range order correlations far above the Néel temperature.

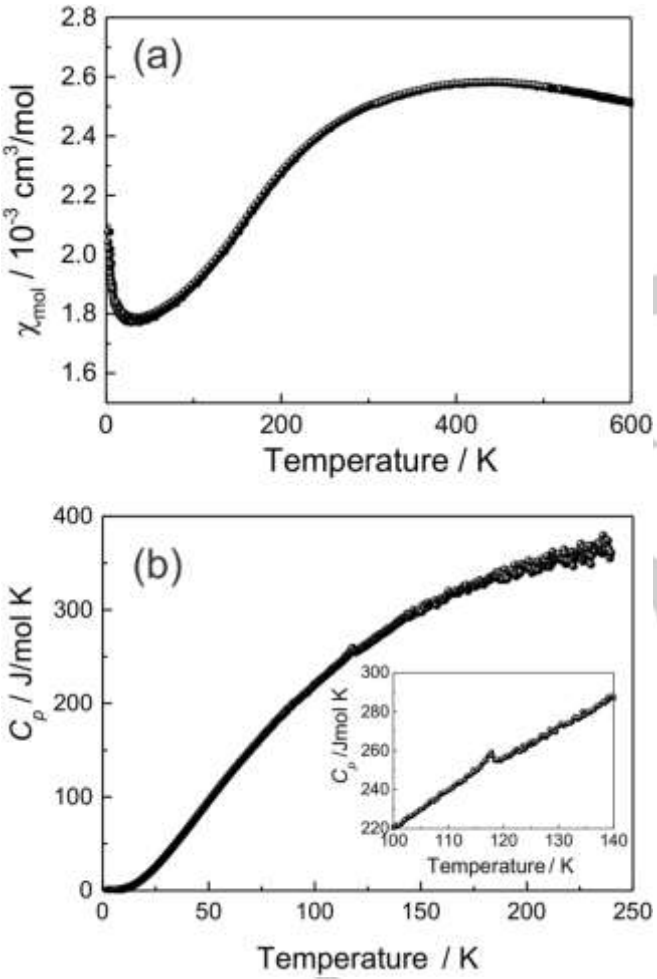

Figure 4. (a) Molar magnetic susceptibility (per one Mn atom) of $K_6Mn_4O_7$ measured in an external field of 1 Tesla. Displayed are zero-field cooled and field cooled data being identical within experimental resolution. (b) Molar heat capacity of $K_6Mn_4O_7$. The inset shows an enlargement of the temperature range around the anomaly at 117.5 K.

In order to extract relevant spin exchange parameters we fitted the magnetic susceptibility to various models. These were considered after a closer inspection of the crystal structure with respect to probable superexchange paths. Figure 5 displays a section of the crystal structure of $K_6Mn_4O_7$ showing the Mn^{2+} cations and O^{2-} anions where we have plotted only such Mn—O—Mn bridges with bond length (Mn—O) between 200 and 212 pm and bonding angles substantially larger than 90°.

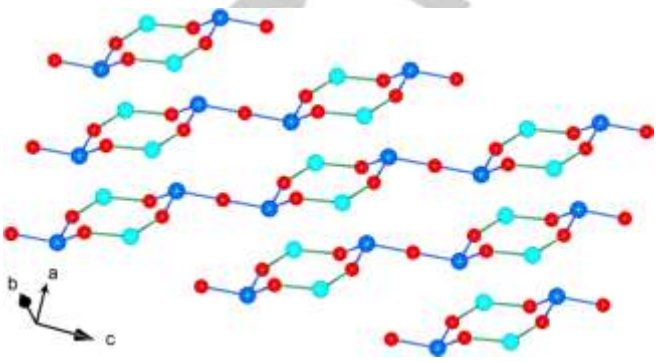

Figure 5. Section of the crystal structure of $K_6Mn_4O_7$ highlighting Mn and O atoms only. The Mn atoms on the two sites are displayed as blue (Mn2) and cyan (Mn1) spheres, respectively. The O atoms are shown in red.

Guided by the Goodenough-Kanamori-Anderson (GKA)[25,26] rules we expect that the 180° Mn2—O—Mn2 bonds between Mn^{2+} cations (see Figure 5) mediate a very strong antiferromagnetic spin exchange, whereas the spin exchange through O^{2-} anions between unlike Mn^{2+} cations via bonds with Mn1—O—Mn2 bond angles ranging between 138° and 157° will still be antiferromagnetic but weaker. These considerations suggest a one dimensional chain as shown in Figure 6 being adequate to describe the magnetic properties of $K_6Mn_4O_7$.

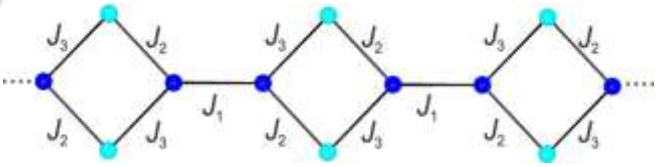

Figure 6. Relevant antiferromagnetic spin exchange coupling pathways, J_1, J_2, and J_3 in $K_6Mn_4O_7$. J_1 involves the 180° bond between Mn2 atoms and an intermediate O atom.

Figure 6 implies the following spin exchange Hamiltonian

$$\mathcal{H} = J_1 \sum_i \vec{S}_{3i-2}\vec{S}_{3i-1}$$
$$+J_2 \sum_i (\vec{S}_{3i-1}\vec{S'}_{3i} + \vec{S}_{3i+1}\vec{S''}_{3i}) + J_3 \sum_i (\vec{S}_{3i-1}\vec{S''}_{3i} + \vec{S}_{3i+1}\vec{S'}_{3i}), \quad (1)$$

where *S* = 5/2 for the Mn^{2+} cations and the spin exchange parameters have been specified in Figure 6.

Equation (1) describes a one dimensional chain with every Mn2 spin moment coupled to two Mn1 moments via the spin exchange parameters J_2 and J_3, the latter most likely smaller than J_1

10.1002/zaac.201800169

coupling Mn2 atoms. Assuming a Heisenberg-type spin Hamiltonian and neglecting exchange anisotropy is justified because of the spin-only moment of the Mn^{2+} cations.

Given that the magnetic susceptibility is essentially governed by a broad hump it seems unlikely that a full fit of eq. (1) results in meaningful spin exchange parameters. We have therefore tried the following approach: We fitted the magnetic susceptibility to linear chain models with (a) uniform nearest-neighbor and (b) with alternating antiferromagnetic spin exchange described by the following alternating chain Hamiltonian

$$\mathcal{H} = J_{nn} \sum_i \vec{S}_{2i-1}\vec{S}_{2i} + J_{nnn} \sum_i \vec{S}_{2i}\vec{S}_{2i+1} = J_{nn} \sum_i (\vec{S}_{2i-1}\vec{S}_{2i} + \alpha\, \vec{S}_{2i}\vec{S}_{2i+1}) \quad (2)$$

where J_{nn} and J_{nnn} represent nearest and next-nearest neighbor spin exchange interactions, respectively, and the alternation parameters is given by $\alpha = J_{nnn}/J_{nn}$. J_{nn} can be identified with J_1 in eq. (1), whereas J_{nnn} averages over J_2 and J_3. For α = 1 one retrieves the uniform chain for which a Padé approximant of precise quantum Monte Carlo calculations is available.[27] Alternating chain quantum Monte Carlo calculations for discrete ratios $0 \leq \alpha \leq 1$ have been reported.[28]

The experimental data were fitted to the general equation

$$\chi(T) = (1-\delta)\chi_{spin}(T) + \delta\chi_{imp}(T) + \chi_0, \quad (3)$$

where the first term describes the spin susceptibility of the uniform or the alternating chain, the second term allows for possible impurities, for which we assumed a Curie-Weiss behavior, and the third temperature independent term comprises diamagnetic contributions from the electrons in the closed shells and temperature-independent paramagnetic Van Vleck susceptibility contributions, the latter being negligible in the half 3*d* shell configuration. The diamagnetic contribution from the closed electronic shell can be estimated from Pascal's increments, Mn^{2+}: -10×10^{-6} cm^3/mol, K^+: -13×10^{-6} cm^3/mol, and O^{2-}: -12×10^{-6} cm^3/mol.[29] With the appropriate number of atoms per formula unit the diamagnetic increments add up to $\chi_{dia} = -202\times10^{-6}$ cm^3/mol per formula unit, i.e. -50.5×10^{-6} cm^3/mol per one Mn atom. In the fits χ_0 was treated as a fitting parameter.

Figure 7 shows fits of equation (3) to the experimental data for a chain with uniform (α = 1) antiferromagnetic spin exchange as well as fits for α = 0.9 and 0.8. The relevant fitting parameters are summarized in Table 4.

Despite the approximate character of eq. (2) the fits are suited to describe the broad susceptibility maximum very well. The spin exchange parameters along the chain are antiferromagnetic and in thermal energy $k_B\times T$ close to 100 K. Deviations from the fit set in below ~200 K, where correlations due to interchain spin exchange may become relevant. An unequivocal sign of long-range magnetic order is neither found in the heat capacity nor in the magnetic susceptibility data underpinning our interpretation of $K_6Mn_4O_7$ as a complex magnetic chain system. The temperature independent contribution, χ_0, obtained from the fit for δ = 1 was found to be $-415(5)\times10^{-6}$ cm^3/mol, considerably larger than expected from the summation of Pascal's increments. The reason for this significant enhancement is currently unknown. The upturn at low temperatures can be attributed to an impurity of less than 0.3% of *S* = 1/2 species following a Curie-Weiss law with a Curie-Weiss temperature between –6 and –4 K.

Table 4. Relevant fit parameters as obtained by fits of eq. (3) to the magnetic susceptibility data.

α	g	$J_{nn}\times k_B^{-1}$ /K	$J_{nnn}\times k_B^{-1}$ /K	χ_0 /10^{-6} cm^3/mol
1.0	2	100(1)	100(1)	–415
0.9	2	102.5(7)	92.3(6)	–415
0.8	2	108(1)	86.4(8)	–415

10.1002/zaac.201800169

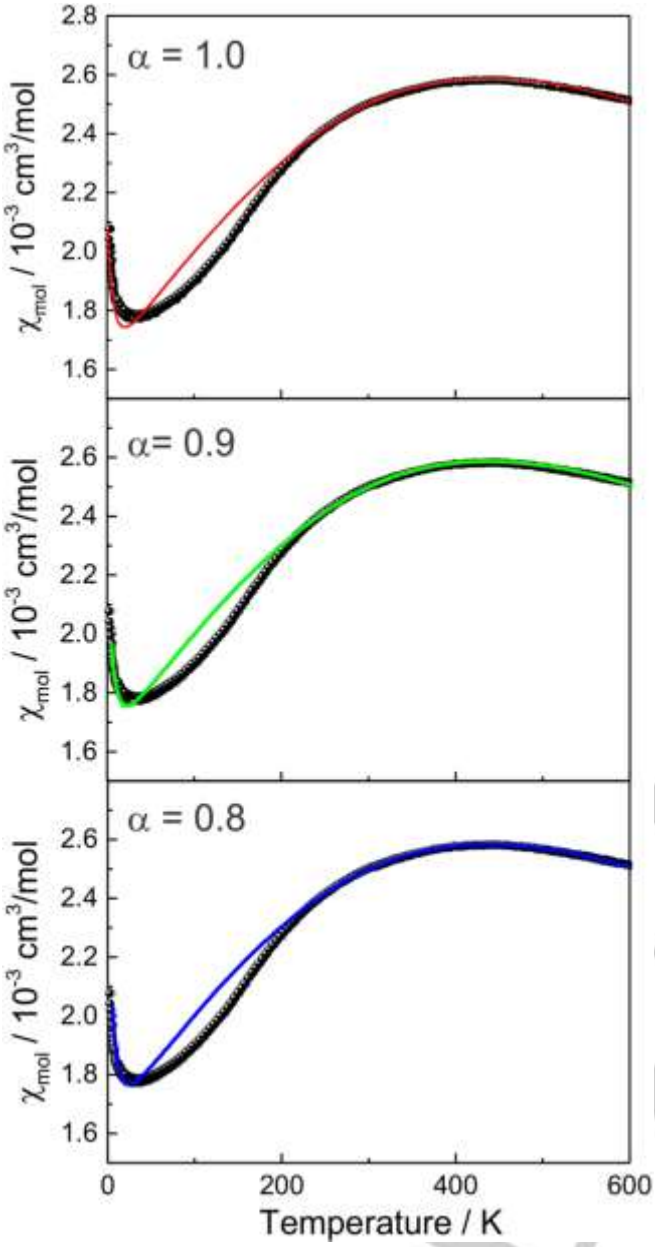

Figure 7. Fits of the magnetic susceptibility of $K_6Mn_4O_7$ with an alternating spin S = 1/2 chain model (eq. 3) with parameters summarized in Table 4 ($\alpha = J_{nnn}/J_{nn}$).

In summary, our semi-quantitative analysis of the magnetic properties of $K_6Mn_4O_7$ guided by the Goudenough–Kanamori rules suggests a description as a one dimensional chain system with antiferromagnetic spin exchange interaction J between S = 5/2 magnetic moments of J/k_B~100 K. Assuming uniform nearest neighbor spin exchange is already sufficient to model the gross features, i. e. the broad maximum centered at ~430 K. This analysis is consistent with the crystal structure featuring chain-like connectivity of building blocks. A further analysis of the various spin exchange paths based on the exact crystal structure is beyond the scope of this paper.

Experimental Section

Synthesis: Phase pure $K_6Mn_4O_7$ can be prepared via the azide/nitrate route[17,18] from MnO, KNO_3 and KN_3. The azide KN_3 was synthesized by distilling HN_3 into an aqueous solution of K_2CO_3.[30] All starting materials were dried at 373 K for 12 h under vacuum (10^{-3} mbar) and mixed in the ratio required according to equation (4).

$$5\ KN_3 + KNO_3 + 4\ MnO \rightarrow K_6Mn_4O_7 + 8\ N_2\uparrow \qquad (4)$$

In a first step, the starting mixtures were ground thoroughly in an agate mortar (~1g batches), pressed to pellets (Ø = 10 mm) under 10^5 N, dried in vacuum (10^{-3} mbar) at 400 K overnight, and placed under argon in closed steel containers, provided with silver inlays. The specially designed containers are equipped with squeeze seals, which withstand the internal pressure to a certain degree, but also let safely escape the considerable amounts of nitrogen formed during the reaction.[17,18] In a flow of dried argon, the following temperature schedule was applied: 298 K → 533 K (100 K/h); 533 K → 653 K (5 K/h); 653 K → 773 K (20 K/h); annealing for 30 h at 773 K, 773 K → 298 K (20 K/h). The obtained product contains single crystals suitable for X-ray diffraction.

Hazards: Rapid heating or running the reaction in a gastight welded container can lead to a dangerous explosion!

Alternatively, micro-crystalline powders can also be obtained by using appropriate amounts of K_2O and MnO according to equation (5), applying a small excess of potassium oxide (~3%).

$$3\ K_2O + 4\ MnO \rightarrow K_6Mn_4O_7 \qquad (5)$$

The starting materials were mixed in a dry-box (M. Braun, Garching, Germany) under argon atmosphere (< 0.1 ppm O_2, H_2O), ground thoroughly in an agate mortar, and sealed in a tantalum ampoule. The following temperature profile was applied: 298 K → 773 K (100 K/h, subsequent annealing for 130 h); 773 K → 298 K (100 K/h).

$K_6Mn_4O_7$ is very sensitive to humid air and therefore all further manipulations must be run in an inert atmosphere of purified argon.

Physical Properties: Magnetic properties were studied with a Quantum Design MPMS7 SQUID Magnetometer (MPMS, Quantum Design, San Diego, CA). The moisture sensitive sample was sealed in carefully dried SUPRASIL ampoules (Ø = 3 mm) under ~500 mbar helium gas. The magnetization of the quartz glass tube was determined in separate runs and subtracted. The heat capacity of powder samples (m ~ 260 mg) was measured in a home-built fully automated double-shield Nernst adiabatic calorimeter similar to that described in detail by Gmelin *et al.*.[31-33] The sample was encapsulated in Duran glass flasks under ~900 mbar helium atmosphere to enable thermal equilibration and attached with a minute amount of Apiezon N vacuum grease to a sapphire platform which carries a thin-film stainless steel heater and a calibrated Cernox thermometer (CX 1050, Lake Shore Cryotronics, Inc., Westerville OH). The heat capacities of the sapphire sample platform, the glass flask and the vacuum grease were determined in separate runs and subtracted from the total heat capacity.

Structure Determination: A crystal suitable for single-crystal X-ray diffraction (SXRD) was selected in a drybox (M. Braun, Garching, Germany) under an argon atmosphere (< 0.1 ppm O_2, H_2O) and fixed inside a sealed glass capillary. Diffraction data were collected at room temperature (298 K) with a SMART-APEX-I CCD X-ray diffractometer (Bruker AXS, Karlsruhe, Germany) with graphite monochromated MoKα radiation. The reflection intensities were integrated with the SAINT subprogram in the Bruker Suite software package.[34] A multi-scan absorption correction was applied using SADABS.[35] The structure was solved by direct methods and refined by full-matrix least-squares fitting with the SHEXTL software package.[36,37] Experimental details and crystallographic data are given in Tables 1 and 2.

An X-ray powder diffractogram (PXRD) of $K_6Mn_4O_7$ was recorded at room temperature on a Stadi-P powder diffractometer, using MoKα_1 radiation (λ = 70.9300 pm, STOE & Cie GmbH, Darmstadt, Germany). The sample was sealed in a borosilicate glass capillary and the data were collected in the range, $3° \leq 2\theta \leq 30°$. The powder pattern was evaluated by the le Bail profile analysis using the software package TOPAS,[38] see Figure 1.

Acknowledgements

The authors thank *M. Stahl* and *S. Prill-Diemer* for carrying out the synthesis, *E. Brücher* for susceptibility measurements, and *Dr. G. S. Thakur* for performing the Le Bail fit.

Keywords: Azide/nitrat route • Manganese • Magnetic properties • Polyanions • Manganates(II)

[1] E. Saitoh, S. Okamoto, K. T. Takahashi, K. Tobe, K. Yamamoto, T. Kimura, S. Ishihara, S. Maekawa, Y. Tokura, *Nature* **2005**, *410*, 180-183.
[2] M. Sofin, E.-M. Peters, M. Jansen, *Z. Anorg. Allg. Chem.* **2002**, *628*, 2697-2700.
[3] M. Sofin, E.-M. Peters, M. Jansen, *J. Solid State Chem.* **2005**, *178*, 3708-3714.
[4] P. Horsch, M. Sofin, M. Mayr, M. Jansen, *Phys. Rev. Lett.* **2005**, *94*, 076403.
[5] S. van Smaalen, R. E. Dinnebier, M. Sofin, M. Jansen, *Acta Crystallogr., Sect. B* **2007**, *63*, 17-25.
[6] L. Capogna, M. Mayr, P. Horsch, M. Raichle, R. K. Kremer, M. Sofin, A. Maljuk, M. Jansen, B. Keimer, *Phys. Rev. B* **2005**, *71*, 140402(R).
[7] M. Raichle, M. Reehuis, G. Andre, L. Capogna, M. Sofin, M. Jansen, B. Keimer, *Phys. Rev. Lett.* **2008**, *101*, 047202.
[8] L. Capogna, M. Reehuis, A. Maljuk, R. K. Kremer, B. Ouladdiaf, M. Jansen, B. Keimer, *Phys. Rev. B* **2010**, *82*, 014407.
[9] J. Nuss, U. Wedig, M. Jansen, *Z. Kristallogr.* **2011**, *226*, 627-632.
[10] N. Z. Ali, J. Sirker, J. Nuss, P. Horsch, M. Jansen, *Phys. Rev. B* **2011**, *84*, 035113.
[11] S. Pfeiffer, J. Nuss, M. Jansen, *Z. Anorg. Allg. Chem.* **2010**, *636*, 23-29.
[12] S. Pfeiffer, J. Nuss, M. Jansen, *Z. Kristallogr.- New Cryst. Struct.* **2009**, *224*, 377-378.
[13] J. Nuss, S. Pfeiffer, S. van Smaalen, M. Jansen, *Acta Crystallogr., Sect. B* **2010**, *66*, 27-33.
[14] J. Nuss, M. A. Señaris-Rodriguez, P. L. V. K. Dasari, M. Stahl, M. Jansen, *J. Am. Chem. Soc.* **2012**, *134*, 11734-11739.
[15] M. Reehuis, M. A. Señaris-Rodriguez, A. Hoser, B. Keimer, M. Jansen, *Phys. Rev. B* **2013**, *87*, 014426.
[16] J. Nuss, P. L. V. K. Dasari, M. Jansen, *Z. Anorg. Allg. Chem.* **2015**, *641*, 316-321.
[17] D. Trinschek, M. Jansen, *Angew. Chem.* **1999**, *111*, 234-235; *Angew. Chem. Int. Ed.* **1999**, *38*, 133-135.
[18] M. Jansen, *Z. Anorg. Allg. Chem.* **2012**, *638*, 1910-1921.
[19] S. Pfeiffer, M. Jansen, *Z. Anorg. Allg. Chem.* **2009**, *635*, 211-215.
[20] S. Pfeiffer, M. Jansen, *Z. Naturforsch.* **2009**, *64b*, 487-490.
[21] S. Pfeiffer, *Z. Kristallogr. - New Cryst. Struct.* **2009**, *224*, 163-164.
[22] J. Nuss, M. A. Señaris-Rodriguez, S. Klemenz, M. Jansen, *Z. Anorg. Allg. Chem.* **2017**, *643*, 1351-1356.
[23] J. Nuss, M. Jansen, *Z. Anorg. Allg. Chem.* **2012**, *638*, 2201-2204.
[24] E. Seipp, R. Hoppe, *Z. Anorg. Allg. Chem.* **1985**, *530*, 117-126.
[25] J. B. Goodenough in *Progress in Solid State Chemistry* (Ed. H. Reiss), Pergamon Press, New York **1971**, *5*, pp. 145-399.
[26] J. B. Goodenough in *Magnetism and the Chemical Bond*, Interscience, New York **1963**.
[27] J. M. Law, H. Benner, R. K. Kremer, *J. Phys.: Condens. Matter* **2013**, *25*, 065601-065609.
[28] Shichao Hu, M. Johnsson, J. M. Law, J. L. Bettis, Jr., M.-H. Whangbo, and R. K. Kremer, *Inorg. Chem.* **2014**, *53*, 4250 – 4256.
[29] P. W. Selwood in *Magnetochemistry*, Interscience Publishers, Inc., New York **1956**.
[30] G. Brauer, *Handbuch der Präparativen Anorganischen Chemie*, 3rd ed., F. Enke, Stuttgart **1975**, vol.1, p 458.
[31] E. Gmelin, *Thermochimica Acta* **1979**, *29*, 1-39.
[32] E. Gmelin, P. Rödhammer, *J. Phys. E* **1981**, *14*, 223-228.
[33] E. Gmelin, K. Ripka, *Cryogenics* **1981**, *21*, 117-118.
[34] Bruker Suite, Version 2013/1. Bruker AXS Inc., Madison, WI, USA, **2013**.
[35] G. M. Sheldrick, SADABS—Bruker AXS area detetctor scaling and absorption correction, version 2008/1; University of Göttingen, Göttingen, Germany, **2008**.
[36] G. M. Sheldrick, *Acta Crystallogr. Sect. A: Found. Crystallogr.* **2008**, *64*, 112-122.
[37] G. M. Sheldrick, *Acta Crystallogr., Sect. C: Struct. Chem.* **2015**, *71*, 3-8.
[38] TOPAS, Version 4.2.: General profile and structure analysis software for powder diffraction data, Bruker AXS, Karlsruhe, Germany, **2008**.

10.1002/zaac.201800169

WILEY-VCH

ARTICLE

FULL PAPER

$K_6Mn_4O_7$ was obtained via the azide/nitrate route. It crystallizes with triclinic symmetry, and contains a novel two-dimensional poly-oxomanganate(II) anion

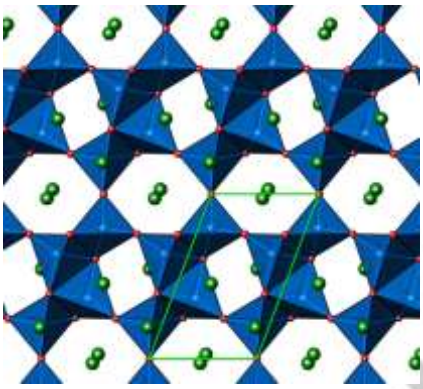

*Jürgen Nuss, Reinhard K. Kremer, and M. Jansen**

Page No. – Page No.

Synthesis, Crystal Structure and Magnetic Properties of $K_6Mn_4O_7$ Featuring a Novel Two-Dimensional Poly-oxomangante(II) Anion

10.1002/zaac.201800169

WILEY-VCH

ARTICLE

Additional Author information for the electronic version of the article.

J. Nuss: ORCID.org/0000-0002-0679-0184
R.K. Kremer: ORCID.org/0000-0001-9062-2361
M. Jansen: ORCID.org/0000-0003-0762-0985